Nanoscale

Accepted Manuscript

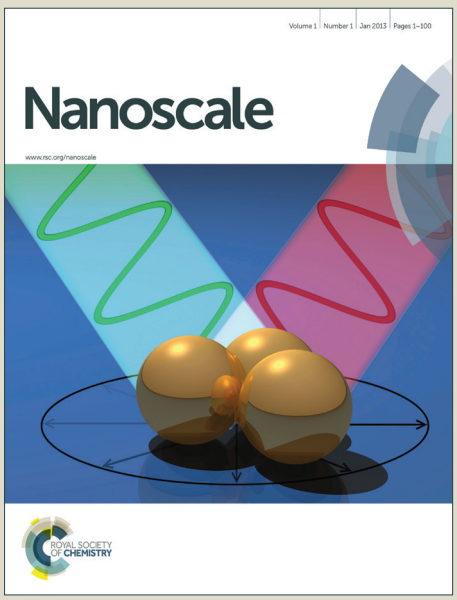

ROYAL SOCIETY OF CHEMISTRY

www.rsc.org/nanoscale

Nanoscale

RSCPublishing

ARTICLE

Self-regulated Route to Ternary Hybrid Nanocrystals Ag-Ag_2S-CdS with Near-Infrared Photoluminescence and Enhanced Photothermal Conversion

Cite this: DOI: 10.1039/xoxxoooooox

Received ooth January 2014,
Accepted ooth January 2014

DOI: 10.1039/xoxxoooooox

www.rsc.org/

Guoxing Zhu,*[a, b, d] Chunlin Bao,[a] Yuanjun Liu,[c] Xiaoping Shen,*[a] Chunyan Xi,[a] Zheng Xu,[d] and Zhenyuan Ji[a]

Developing hybrid nanocrystals is a hot topic in material science. Herein, a ternary hybrid nanocrystal, Ag-Ag_2S-CdS, combining near infrared emission and photothermal conversion properties was demonstrated. The ternary Ag-Ag_2S-CdS hybrid nanocrystals with cubic shape and uniform size were synthesized by a simple one-pot and one-step colloidal method. The growth process is self-regulated with the formation order of Ag_2S, Ag, CdS, respectively. The formation of Ag originates from the partial reduction of Ag_2S, while the formation of CdS is through an Ag_2S catalytic mechanism based on its superionic feature. The obtained ternary hybrid nanocrystals show near infrared emission and photothermal conversion properties in the lab-on-a-particle system. Importantly, an enhanced effect is observed for the photothermal conversion, which is mainly due to the presence of heterointerfaces among them. This work will not only advance the synthesis chemistry of multi-component hybrid nanocrystals but also provide a possible route for the design of advanced multi-model materials used in bio-related fields.

Introduction

As one interesting emerging class of colloidal nanostructures, hybrid nanocrystals combine two or more chemically disparate components into one entity, providing a powerful approach for bottom-up design of novel micro-/nanoarchitectures and integrating the multifunctions and properties from the individual components.[1] These unique, hybrid lab-on-a-particle systems with clean and intimate solid-state interfaces support direct electronic and magnetic communication between components, which is difficult for the physical mixture systems or nanocomposites assembled by using molecular linkers.[2] Thus some novel synergistic effects are often observed in these hybrid nanocrystals, especially those composed of semiconductor or metal.[3] Up to date, some pioneering cases[4-14] have been reported in recent years including CdSe/Au,[4-5] Fe_3O_4/Au,[6] ZnO/Au,[7] Ag_2S/Au,[8] In_2O_3/FePt,[9] Ag_2S/Ag,[10,11] $Cu_{1.94}S$/CdS,[12] Fe_2O_3/II-IV sulfide,[13] Ag_2S/CdS.[14] However, the reported hybrid nanocrystals are mainly focused on binary system, few reports about the construction of ternary or higher-order hybrid nanocrystals.[2] In the synthesis process, a multistep route and the try-and-error method were often adopted to search the optimum experiment parameters such as temperature, solvents, surfactants (including the types, concentrations, even rigorous combination of two or more different ones), concentration of the precursors, feeding way, and so on, which is tremendously trivial and tedious. Thus, a facile one-step or one-pot route is highly preferred for the synthesis of multi-model hybrid nanocrystals.

As for functional nanomaterials applied in bio-related areas, near infrared emission and photothermal conversion are two hot topics.[15-17] Near-infrared ray (NIR, λ = 700-1100 nm) can penetrate biological tissues with less interference from blood and tissue autofluorescence,[18] thus the materials with near infrared emission are often used as bio-imaging agent for bio-labeling.[19-24] Materials with photothermal conversion property can transfer the laser energy into heat,[25-33] which is able to burn tumors. Integrating a photothermal agent and a near infrared emission component into one single hybrid nanoparticle would be useful for their bio-related application.[34, 35]

Ag nanocrystals have attracted considerable attention mainly as a result of their remarkable properties and numerous applications in fields such as biological antimicrobial, surface plasmonics, surface-enhanced Raman scattering, and chemical or biological sensing. Ag_2S is a high chemical stability, direct narrow-band-gap (0.9-1.1 eV) semiconductor. It also has a relatively large absorption coefficient and good thermal performance.[36-39] Furthermore, Ag_2S shows an excellent near infrared emission[38, 39] and is an effective supersonic semiconductor in which Ag^+ ions behave like free electrons in

metals resulting in rich cationic vacancy. Such unique chemical and structural properties endow it as an excellent host mediator/catalyst for preparation of Ag_2S-based hybrid nanocrystals with improved properties.[40-45]

Herein, a convenient, one step and one pot method was devised for the synthesis of a new type ternary hybrid nanocrystals composed of Ag-Ag_2S-CdS. The reaction process is self-regulated with the sequential formation of Ag_2S, Ag, CdS, respectively. Our synthetic protocol with one-pot and one-step self-regulated reaction greatly simplifies the general preparation of hybrid nanocrystals, it does not need hot injection, no require of high temperature. Importantly, these new Ag-Ag_2S-CdS hybrid nanocrystals exhibit both fluorescence emission at NIR region and enhancement effect in photothermal conversion performance. The results presented here may not only contribute to the fabrication methodology, but also give some hints for the future exploitation of multifunction hybrid nanocrystals applied in biology fields.

Experimental

Materials

The chemical reagents employed in this research are A. R. grade and were purchased from Sinopharm Chemical Reagent Co. China. Oleylamine (C_{18}:80-90%) (OLA) and octadecylamine was purchased from Aladdin Industrial Corporation (Shanghai, China). All reagents were used as received without further purification.

Synthesis of $Cd(ddtc)_2$ (ddtc = S_2CNEt_2) precursor

Cadmium (II) diethyldithiocarbamate was prepared based on a previously published procedure.[40] Typically, NaOH (2.64 g) and *n*-diethylamine (11 mL) were added to methanol (80 mL) under ice-water bath condition. Then CS_2 (3.96 mL) was added into the mixture dropwise. After that, the obtained yellow solution was mixed with aqueous solution of $CdSO_4$ (80 mL, containing 9.5 g of $CdSO_4 \cdot 8H_2O$) and stirred vigorously for at least 3 h. The yellow solid product, $Cd(ddtc)_2$, was separated by filtration, washed with water for several times, and dried at room temperature.

Synthesis of Ag-Ag_2S-CdS heteronanostructures

Typically, AgI (0.031 g) and $Cd(ddtc)_2$ (0.023 g) (Ag/Cd = 0.42) were firstly dispersed in 5 mL of oleylamine with vigorously stirring. The resulting mixture was then heated to 150 ^oC with a rate of about 10 ^oC/min and kept at that temperature for 0.5-1 h. After the reaction system was cooled to room temperature, the black product (Ag-Ag_2S-CdS) was collected by centrifugation and washed for at least three times with cyclohexane and absolute ethanol for further characterization.

Synthesis of Ag_2S, CdS, Ag nanocrystals

The synthesis of spherical Ag_2S nanocrystals follows on previously published procedure.[46] Octadecylamine (20 g) was firstly heated to 120 ^oC, forming a colorless transparent liquid. Then $AgNO_3$ (0.2 g) and S powder (60 mg) were added to the hot octadecylamine sequentially. After the addition of S powder, the color of the mixture changed from turbid yellow to brownish black, indicating the formation of Ag_2S nanocrystals. With further reaction for 1 h at 120 ^oC, the resulting Ag_2S nanocrystals were collected by centrifugation, washed several times with ethanol, $CHCl_3$ and cyclohexane, respectively. The precipitate was dispersed in cyclohexane for later characterization. For CdS nanocrystals, $Cd(ddtc)_2$ (0.023 g) and oleylamine (5 mL) were added in a three-necked flask with magnetic stirring. The reaction system was then heated to 150 ^oC and reacted for 1 h. The CdS nanocrystals were precipitated with ethanol as a bad solvent. After being washed by ethanol and cyclohexane for several times, CdS nanocrystals were dispersed in cyclohexane for further characterization. Ag nanocrystals were also prepared on a reported method.[47]

The photothermal conversion test for cancer cells in vitro

The photothermal effect test *in vitro* was carried out by a method similar to references.[31, 33] The Ag-Ag_2S-CdS nanocrystals were firstly treated through ligand exchange with 6-amino caproic acid to transfer it to be hydrophilic state. Briefly, a certain amount of Ag-Ag_2S-CdS nanocrystals were dispersed into the mixture of hexane (35 mL), distilled water (15 mL), and ethanol (30 mL) through magnetic stirring. Then, 6-amino caproic acid (0.13 g) and equivalent molar $NH_3 \cdot H_2O$ in 5 mL of distilled water was added into the above system. After that, the mixture was heated to 70 ^oC and kept at that temperature for 4 h. The nanocrystals were collected by centrifugation. Through this process, the hydrophobic hybrid nanocrystals were transformed into hydrophilic state, which can be dispersed in water.

For the *in vitro* cancer cell experiment, phosphate buffer solution (PBS) dispersions containing 0.03 mg/mL of hybrid nano-crystals or PBS controls were added into the cell plate. After irradiating by a 980 nm NIR laser with an output power density of 0.5 W for 3 min. The cells were further incubated for 10 h. A 3-(4,5-dimethylthiazol-2-yl)-2,5-diphenyltetrazolium bromide (MTT) assay was then used to calculate the cell viability.

Characterizations

Powder X-ray diffraction (XRD) measurements were carried out on an X-ray diffractometer (Bruker D8 Advance diffractometer) with Cu Kα radiation. The morphology and size of the products were examined by a transmission electron microscope (TEM, JEOL JEM-2100) with an accelerating voltage of 200 kV. Fast Fourier transform (FFT) algorithms were performed using DigitalMicrograph software. Energy-dispersive X-ray spectrum (EDS) was also performed on a JEOL-2100 microscope. The product dispersed in cyclohexane was dropped onto a holey copper grid covered with an amorphous carbon film for the TEM examination of morphology. The valence of the elements in the sample was detected by X-ray photoelectron spectroscopy (XPS, Thermo ESCALAB 250) with $Al_{K\alpha}$ (hν = 1486.6 eV) X-ray radiation source. The XPS spectrum was calibrated by C 1s peak (284.6 eV). The optical properties of the samples were recorded from the cyclohexane dispersion using an UV-3000 Spectrophotometer or a Shimadzu UV-VIS-NIR Spectrophotometer (UV-3600) and a QuantaMaster & Time Master Spectrofluorometer (QuantaMaster™ 40).

For measuring the photothermal conversion performances of these samples, 980 nm near infrared (NIR) laser was delivered through a glass cuvette containing cyclohexane dispersion (1 mL) of the samples with different concentrations. The light source is a 0.5 W, 980 nm semiconductor laser device with a 6 mm diameter laser module (Ningbo Ruanming Laser Technology Co., Ltd. China). A thermocouple was inserted into the cyclohexane dispersion of the tested sample perpendicular to the path of the laser for recording the change of real-time temperature. The temperature was recorded per 20 s.

Results and Discussion

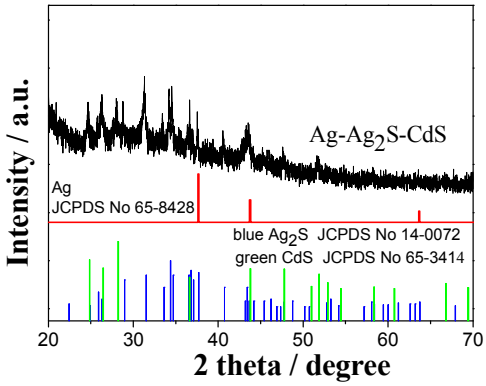

Fig. 1 XRD pattern of the as-prepared Ag-Ag_2S-CdS hybrid nanocrystals accompanied with standard JCPDS cards of Ag_2S (No. 14-0072), CdS (No. 65-3414), and Ag (No. 65-8428) for comparison.

Synthesis and Characterization The three component Ag-Ag_2S-CdS hybrid nanocrystals were synthesized by a one-pot and one-step colloidal route. Oleylamine was employed as the growth solvent and capping agent. AgI and $Cd(ddtc)_2$ were used as the reactants and both were directly dispersed in oleylamine. Direct heating of the reaction system induces the formation of Ag-Ag_2S-CdS hybrid nanocrystals. Figure 1 shows the XRD pattern of the colloidal hybrid nanocrystals, which confirms that the as-prepared sample consists of Ag_2S with monoclinic phase structure (JCPDS Card No. 14-0072) and CdS with hexagonal phase structure (JCPDS Card No. 65-3414), while the diffraction peaks from silver overlap with that of Ag_2S or CdS.

The morphology, structure, and size of the hybrid nanocrystals were characterized by TEM, which reveals that the sample is composed of uniform nanoparticles with cubic shape and good monodispersity (Figure 2a, b). The spacing between nanoparticles is ~2.9 nm due to the presence of the capped surfactant molecules, oleylamine, which also gives the particles a good dispersibility in non-polar solvents such as cyclohexane and $CHCl_3$. From the TEM image with higher resolution (Figure 2b), distinct interface and different contrast are observed in each cubic particle, suggesting that the particles contain multiple components.

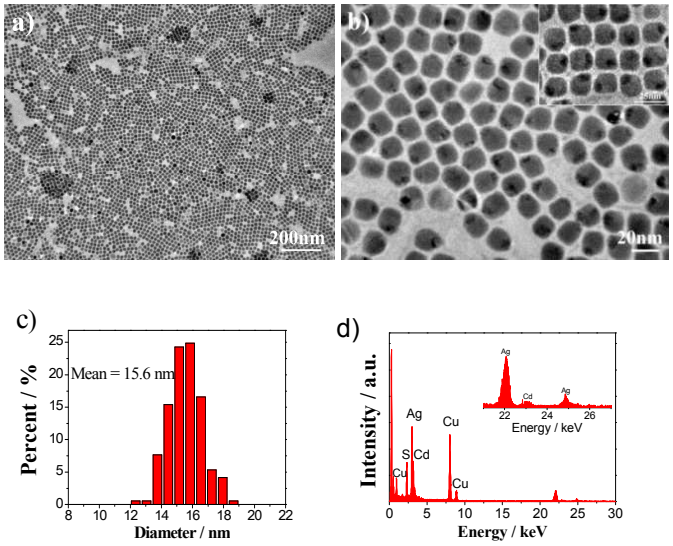

Fig. 2 a, b) TEM images, c) size distribution and d) EDS spectrum of the as-prepared Ag-Ag_2S-CdS hybrid nanocrystals. The inset of d) shows the corresponding magnified part in the range of 21-27 keV.

The nanoparticles have an average size of 15.6 nm. The good monodispersity of the ternary hybrid nanocrystals was also demonstrated by statistical analysis of size distribution (Figure 2c). The high uniformity of size and shape, as well as the capping of oleylamine endows the self-assembly of the hybrid nanocrystals on carbon film with hexagonal or cubic array (as shown in Figure 2b). The multi-layer self-assembly adopts an ABAB mode and induces the formation of highly ordered microstructure (Figure SI-1, see Supporting Information (SI)). It should be noted that the ordered assembly of hybrid nanocrystals is rarely reported partially owing to the difficulty in synthesis of uniform and regular hybrid nanocrystals.

The composition of the hybrid nanocrystals was firstly determined by EDS equipped on the TEM (Figure 2d), which was conducted on about ten nanoparticles. The EDS results demonstrate that Ag, Cd and S elements are present in the particles. Figure 3 shows the high-resolution (HR) TEM image of an individual cubic nanoparticle with the corresponding fast Fourier transform (FFT) patterns. The image shows three clear and different lattice fringes, corresponding to Ag, CdS, and Ag_2S phase (spacing measure and more images shown in Figure SI-2, see SI). The Ag region has a size of about 4 nm. The interplanar distance of 0.20 nm is detected in the area with higher contrast, attributable to (111) planes of cubic silver. The lattice spacing of 0.35 nm originates from (100) planes of CdS, while that of 0.24 nm is coincident with that of (112) planes of Ag_2S.

The composition of the hybrid materials was further characterized by using XPS analysis. Figure 4 shows the detailed photoelectron region for S 2p, Cd 3d, Ag 3d, and Ag MNN Auger structure. The XPS peaks of S 2p centred at the binding energies of 160.8 and 162.1 were assigned to the Ag-S and Cd-S, respectively (Figure 4a).[48-51] The high-resolution

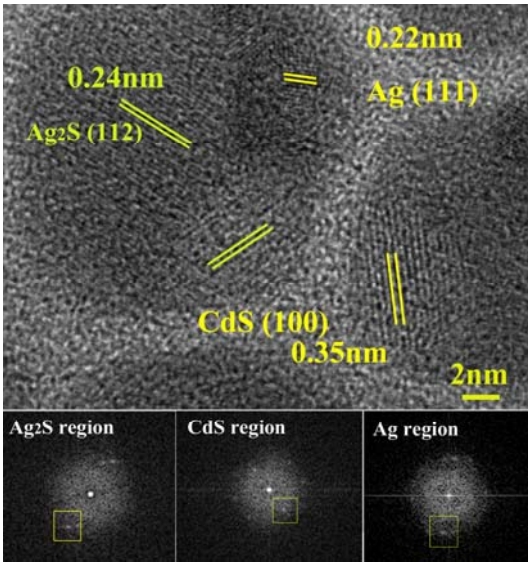

Fig. 3 HRTEM image of an individual hybrid nanocrystal with the corresponding fast Fourier transform patterns.

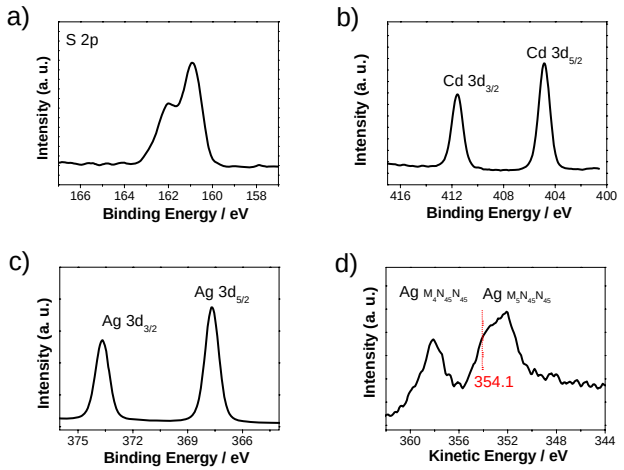

Fig. 4 XPS spectra of a) S 2p, b) Cd 3d, c) Ag 3d, and d) Ag MNN Auger structure.

spectrum of Cd 3d with featured peaks at 411.6 (Cd $3d_{3/2}$), 404.9 eV (Cd $3d_{5/2}$) and spin orbit separation of 6.7 eV reveals the Cd element with +2 oxidation state (Cd^{2+}) (Figure 4b). The binding energies also agree well with the reported XPS spectrum for Cd 3d region in CdS nanoparticles.[49, 52]

In order to determine the chemical environment and oxidation state of silver in the product. We have performed XPS measurement at the Ag 3d region and Ag MNN Auger structure level. The corresponding spectra are showed in Figure 3c and 3d, respectively. The Ag $3d_{5/2}$ and Ag $3d_{3/2}$ core level binding energies appear at 367.7 and 373.7 eV (Figure 3c). While these two peaks were not helpful to characterize the oxidation state of silver, as metallic silver 3d peaks have almost identical value to that of Ag^+ species (the reported Ag $3d_{5/2}$ in the range of 367.9-368.4 eV for Ag^0, 367.6-368.5 eV for Ag^+).[50, 53] Fortunately, the Auger peaks of silver allow reliable distinguishing the metallic form (Ag^0) from the oxidized forms through modified Auger parameter. As shown in Figure 3d, the Auger structure of silver shows peaks at 358.2, 354.1, and 352.1 eV. Among them, the obvious shoulder peak at 354.1 eV is consistent with Ag^+ species such as Ag_2SO_4 (354.2 eV),[54] suggesting Ag^+ is involved in the sample. The modified Auger parameter for the peaks of 358.2 and 352.1 is calculated to be 725.9 and 719.8 (calculated by adding binding energy of Ag $3d_{5/2}$ and Kinetic energy of Auger, here, 367.7+358.2 or 367.7+352.1, respectively). These two values agree well with that of metallic silver (726.3, 720.3),[50, 53, 55, 56] revealing the presence of metallic silver in our prepared product. This result shows that silver species with two oxidation states (Ag^0 and Ag^+) are included in the product. From the above analysis based on XRD, EDS, HRTEM, XPS, it is concluded that the hybrid nanocrystals, Ag-Ag_2S-CdS, are obtained.

Growth mechanism Three-component hybrid nanocrystals are rarely prepared by an one-pot and one-step colloidal synthetic approach. Up to date, the synthesis of multi-component hybrid nanocrystals adopts a multi-step growth mode with complex synthesis route. To understand the formation process and growth mechanism of these unusual Ag-Ag_2S-CdS hybrid nanocrystals, the reaction was traced along the heating and reaction process by taking out an aliquot of reaction mixture for TEM analyses (Figure 5). After AgI and $Cd(ddtc)_2$ were mixed together in oleylamine, the solution turned glassy yellow. The reaction proceeded with the increasing of temperature. As the temperature was increased to 80 ^oC, the reaction system was still composed of AgI and $Cd(ddtc)_2$ with sheet-like particles (Figure 5a), as indicated by the corresponding EDS spectrum (Figure SI-3, see SI). Further increasing of reaction temperature will cause the gradual change of the reaction mixture into brown color, suggesting the formation of sulfide nanoparticles. When the temperature reached 140 ^oC, some spherical Ag_2S nanoparticles were formed (Figure 5b), which become the predominant product as the reaction system was heated to 150 ^oC and kept at that for 5 min (Figure 5c). The spherical Ag_2S nanoparticles have a mean size of 17 nm (Figure SI-4a, see SI). The corresponding XRD pattern and HRTEM image reveals the Ag_2S nanoparticles are pure phase (Figure SI-4b, c, see SI), without the presence of Ag or CdS phase. This was further confirmed by EDS spectrum, which shows the absence of Cd element (Figure SI-4d, see SI).

Further prolonging the reaction time to 7 min at 150 ^oC causes the formation of Ag. As shown in Figure 5d, smaller Ag nanoparticles with a diameter of ~4 nm were attached on the spherical Ag_2S nanoparticles. At this stage, the particles are also spherical but with relatively smaller size of 12 nm (Figure SI-5a, see SI). While reacting for 15 min at 150 ^oC, cubic hybrid nanocrystals with high yield were obtained, although some spherical particles also exist (Figure 5e). The cubic hybrid nanocrystals have an average size of 15.9 nm (Figure SI-5b, see SI), which is basically consistent with that obtained with 30 min reaction (Figure 2). This growth process proves that the formation of Ag-Ag_2S-CdS hybrid nanocrystals follows a self-regulated mode "Ag_2S formation → Ag formation on Ag_2S →

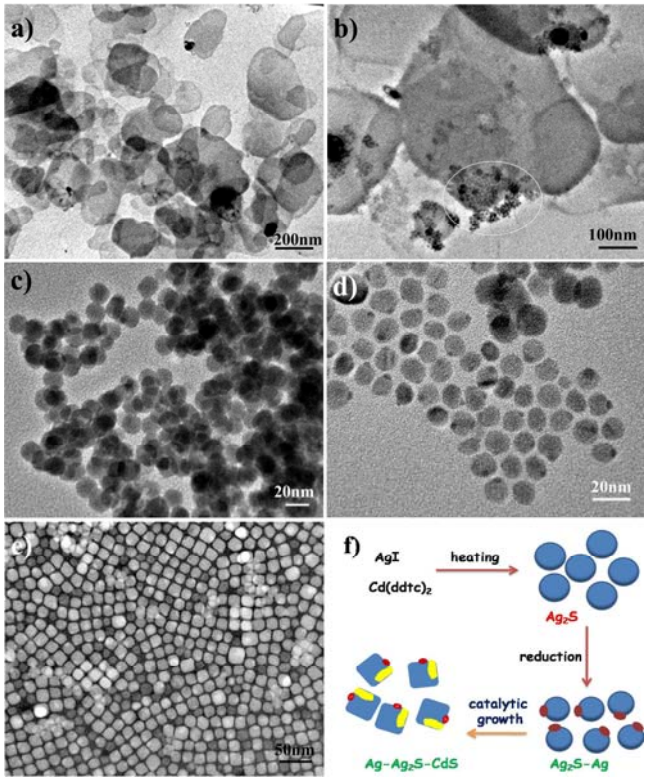

Fig. 5 TEM images showing the growth process of the Ag-Ag_2S-CdS hybrid nanocrystals. The products obtained when the temperature of the system increased to 80 °C (a), 140 °C (b). The formation of spherical nanoparticles is noted by a white circle in (b). The products obtained when the reaction system kept at 150 °C for 5 min (c), 7 min (d), and 15 min (e). e) is an inverse TEM image clearly showing cubic structure with the presence of Ag. f) Schematic of the formation process.

CdS formation". On the other hand, the particle size also undergoes a change, first decreasing from 17 nm of spherical Ag_2S nanoparticles to 12 nm of Ag-Ag_2S, and then increasing to 15.9 nm of Ag-Ag_2S-CdS hybrid nanocrystals. Schematic of the formation process is shown in Figure 5f.

This formation process is also confirmed by an absorption spectroscopy investigation during the heating and reaction process. Figure 6a shows the UV-Vis absorption spectra along the process. There is an obvious absorption at 370 nm before the reaction system was heated to 150 °C, corresponding to that of AgI. The disappearance of that when the reaction system heated at 150 °C for 2 min suggests that AgI is fully reacted at this stage. Figure 6b exhibits absorption spectra of several typical samples in the Vis-NIR range, in which the absorption of Ag_2S locates.[38, 39] A weak should peak at around 840 nm is detected after the reaction mixture was heated to 140 °C, suggesting Ag_2S is formed at this stage. It seems the entire absorption starts from about 1200 nm. The result from absorption spectrum analysis is consistent with the TEM observation.

Based on the observed experimental results, a formation mechanism of this unique ternary hybrid nanocrystals was proposed. Firstly, AgI reacts with $Cd(ddtc)_2$ forming spherical Ag_2S nanoparticles with size of 17 nm, in which the ligand of *ddtc* provides the sulfur source. Then, Ag-Ag_2S hybrid nanocrystals are formed with the particle size decreasing from 17 nm to 12 nm, implying the Ag nanocrystals deposited on Ag_2S come from the partial reduction of Ag_2S, possibly by I^-, oleylamine, or sulfur derivatives. That metalic Ag clusters form in sulfide system is also reported in previous studies.[57-60] For example, Urban *et al* found that polycrystalline silver metal clusters are produced during Ag_2S nanocrystals growth, even through in the reaction system the sulfur source is highly excess. It is widely proposed that sulfur ion vacancies at the Ag_2S nanocrystal surface, the catalytic role of Ag_2S, and the high Ag^+ mobility in Ag_2S favor the reduction of Ag^+ ions coming from the internal structure of Ag_2S nanocrystals.[58-60]

Once an Ag nanocluster is formed on the surface of Ag_2S, Ag-Ag_2S junction is formed. This metal-semiconductor junction will induce the electron transfer from Ag_2S to Ag driven by equilibration of the Fermi energy (Figure SI-6, see SI).[61, 62] There are several well-known examples of strong metal-semicondutor interactions characterized by electron transfer from the semiconductor to metal, significant change in surface chemistry and chemical reactivity.[63, 64] This electron transfer enhances the stability of Ag_2S and prevents Ag_2S from being further reduced. The relatively stable Ag-Ag_2S hybrid nanocrystals guide the succedent growth of CdS phase.

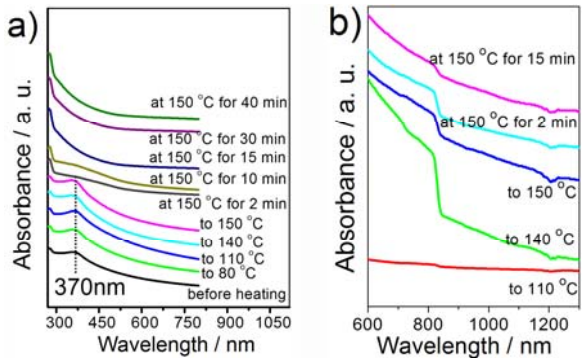

Fig. 6 Absorption spectra of the reaction products extracted during the heating and reaction process in a) the Uv-Vis region and b) the Vis-NIR region.

It is believed that the formation of CdS phase in the hybrid nanocrystals follows a catalytic growth mechanism and induces the structural transformation of spherical particles to cube. Monoclinic Ag_2S is a ionic conductor with high cationic mobility. At the reaction temperature, Ag_2S would be superionic phase owing to the smaller nanoscale size and therefore has more cationic vacancies,[40, 42, 43, 65] which are favorable for Cd^{2+} cation incorporation. The continual transport and incorporation of Cd and S species from solution into the preformed Ag_2S catalyst leads to the formation of Ag-Cd-S solid solution in superionic phase Ag_2S nanoparticles; when it reaches supersaturation, phase separation occurs; CdS is precipitated from the solid solution forming Ag-Ag_2S-CdS hybrid structure.[40] The proposed catalytic growth model displays the characteristic feature similiar to that of vapor-

liquid-solid (VLS) and solution-liquid-solid (SLS) models, but is quite different from the seeded growth.[40, 42] There is an incorporation step followed by phase separation process, unlike the seeded growth mechanism where the second component grows directly on the active facet of seeds. During the incorporation and the subsequent phase separation process, the catalyst particles re-structure, which induces the formation of a distinct heterointerface and often causes the shape change of catalyst particles. In our case, the incorporation of Cd/S species into Ag-Ag_2S induces the particle shape changing from being spherical into cubic. And owing to the introduction of Cd/S components, the size of the hybrid nanocrystals increases from 12 nm to 15.9 nm.

In this synthesis, AgI is necessary for the formation of uniform hybrid nanoparticles. If AgI was replaced with $AgNO_3$ or AgCl, no cubic three-component hybrid nanocrystals were obtained (Figure SI-7, see SI). Presumably, the strong bonding action of I^- to Ag modulates the reaction kinetics, causing the self-regulated formation of uniform hybrid nanoparticles. It seems that the rising rate of temperature is critical for the final product. Decreasing the heating rate to 3 ^oC/min, the product is homogenerous phase particles (Figure SI-8a, See SI). It should be noted that a moderate temperature (such as 150 ^oC) is also necessary for the synthsis of the tertary hybrid nanocrystals. If with higher temperature (higher than 180 ^oC), irregular sub-micrometer spheres were obtained (Figure SI-8b, See SI).

It was found that the molar ratio of Ag/Cd also influences the formation of Ag-Ag_2S-CdS hybrid nanocrystals. By decreasing the molar ratio of AgI/Cd(ddtc)$_2$ to 1:0.92, as shown in Figure SI-9 (see SI), monodisperse nanocrystals with ellipsoid structure were obtained. The corresponding XRD pattern suggests that they are composed of Ag_2S and CdS phases (Figure SI-10a, see SI). Statistical analysis gives the mean diameter of 16.0 nm for the Ag_2S-CdS hybrid nanocrystals (Figure SI-10b, see SI). The HRTEM image reveals that no Ag particles attached on the Ag_2S-CdS hybrid nanocrystals. Interestingly, it seems that the Ag_2S and CdS phases distribute interlacedly in these hybrid nanocrystals.[14] If further decreasing the molar ratio to 1:1.37 or 1:1.84, a mixture of various nanostructures was obtained (Figure SI-11a, b, see SI). While with higher molar ratio of Ag/Cd (1: 0.14), that is, Cd species is relatively lower, spherical hybrid nanoparticles were obtained (Figure SI-11c, see SI).

Optical properties To inspect the quantum confinement effect of the Ag-Ag_2S-CdS hybrid nanocrystals, their optical properties were further investigated by using ultraviolet-visible-near-infrared (UV-Vis-NIR) absorption spectroscopy and photoluminescence spectroscopy (PL). Figure 7a shows the UV-Vis-NIR absorption spectrum of the Ag-Ag_2S-CdS hybrid nanocrystals. The shoulder peak at ~500 nm in the absorption spectrum is attributed to the absorption of CdS. No sharp excitonic absorption of CdS is observed, which is possibly due to the hybrid nanostructures known to change the optical properties.[66, 67] Similar phenomena was observed in the CdS-PbS hybrid system. In that case, the sharp excitonic absorption of CdS gradually becomes to should peak when PbS is attached on them.[67] Possibly owing to the relatively strong absorption of CdS in the spectrum, the absorption of Ag_2S is difficult to distinguish.[68] Magnifing the absorption in the range of 600-1300 nm, it can seen that the adsorption onset is about 1200 nm. A weak absorption peak at 845 nm is also discernible. The absorption in this range would relate to the defect levels or excitonic absorption of Ag_2S. The absorption is lower than that of Ag_2S quantum dots (920 nm),[38] and shows an obvious blue-shift relative to the band-gap energy of bulk Ag_2S (E_g = 0.9-1.1 eV), implying that the Ag_2S phase in the hybrid nanocrystals behaves within the quantum-confinement region.[69]

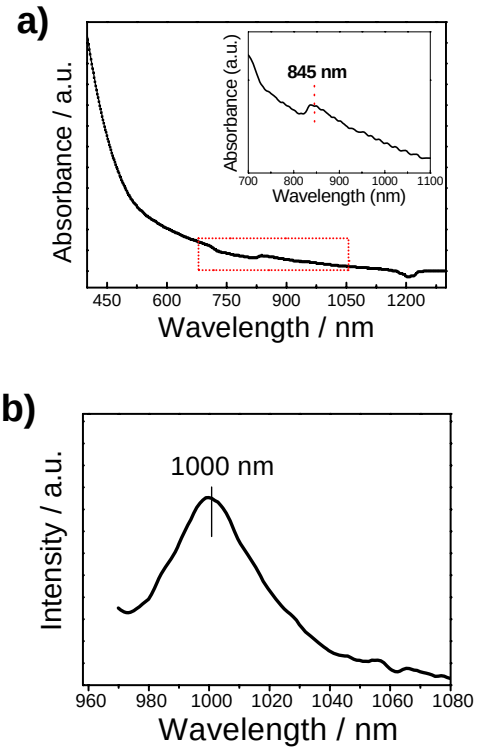

Fig. 7 a) UV-Vis-NIR absorption spectrum and (b) PL spectrum of the Ag-Ag_2S-CdS hybrid nanocrystals in $CHCl_3$. The inset of a) shows the corresponding magnified spectrum. The PL spectrum was taken with 924 nm excitation.

It is well known that Ag_2S nanocrystals show NIR emission.[70] Figure 7b depicts the NIR photoluminescence spectrum of the Ag-Ag_2S-CdS hybrid nano-structures excited with a 924 nm laser. A symmetric emission peak centered at ~1000 nm was observed with a full width at half-maximum (FWHM) about 20 nm. This narrow FWHM could be attributed to the narrow size distribution of the Ag-Ag_2S-CdS hybrid nanocrystals. It seems that the hybrid structures show little influence on the NIR emission position from Ag_2S phase (Figure SI-12, see SI). These NIR fluorescent nanoparticles would be of great interest for *in vivo* bio-imaging, because the fluorescence they emit could penetrate deeply into the body and is poorly absorbed by hemoglobin and water in the body.[71, 72]

Photothermal conversion The absorption of the Ag-Ag_2S-CdS hybrid nanocrystals at NIR region would result in temperature increase of the surrouding medium, since NIR

irradiation has a strong thermal effect.[73, 74] The previous study by Wang *et al* also indictaes that the photo-absorption of Ag_2S would posssibly induce a heat effect.[75] To demonstrate this, we investigated the photothermal conversion capability of Ag-Ag_2S-CdS hybrid nanocrystals and compared it with that of similar-sized Ag_2S nanoparticles at the same concentration. The TEM image of Ag_2S nanoparticles is shown in Figure SI-13 (see SI). The photothermal conversion test was conducted under the irradiation of 980 nm laser. The corresponding results are shown in Figure 8. Controlled experiment shows that the temperature increase of pure solvent (cyclohexane) is less than 0.5 °C in 5 min irradiation. In contrast, in the presence of the Ag-Ag_2S-CdS hybrid nanocrystal the temperature elevation is 4.7 °C in 5 min, which is much higher than that of Ag_2S with similar size (2 °C). With the same test conditions, the temperature elevations of Ag and CdS nanoparticle dispersions are 2.5 and 0.5 °C, respectively. This suggests that the photothermal conversion efficiency can be significantly improved with the formation of hybrid nanocrystals.

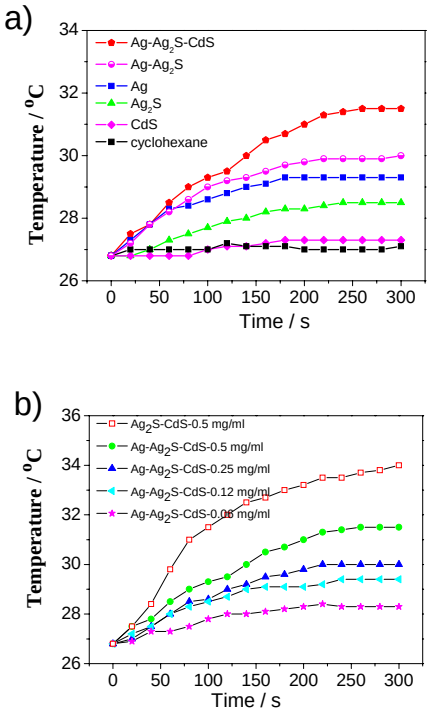

Fig. 8 a) The temperature elevation of the cyclohexane dispersions containing the Ag-Ag_2S-CdS, Ag-Ag_2S hybrid nanocrystals, Ag, Ag_2S, CdS and pure cyclohexane (control experiment), respectively, with the concentration of 0.5 mg/ml as a function of irradiation time of 980 nm laser. (b) The temperature elevation of the cyclohexane dispersion of Ag-Ag_2S-CdS and Ag_2S-CdS hybrid nanocrystals with different concentration as a function of irradiation time.

As shown in Figure 8b, the Ag_2S-CdS product (shown in Figure SI-9) causes the biggest temperature increase (7.2 °C), which is much higher than that of pure Ag_2S and CdS, indicating the positive effect of the formation of Ag_2S/CdS heterointerfaces on the photothermal conversion. For further studying the effect of Ag-Ag_2S heterointerface, we then tested the obtained Ag-Ag_2S nanocrystals (shown in Figure 5d) with the same concentration, which is shown in Figure 8a. It can be seen that the temperature increase of Ag-Ag_2S product is higher than that of Ag, Ag_2S, but lower than that of Ag-Ag_2S-CdS hybrid nanocrystals. This reveals the promoting effect of Ag/Ag_2S, Ag_2S/CdS heterointerfaces on the photothermal conversion.

The photothermal conversion capabilities with the different concentrations of the Ag-Ag_2S-CdS hybrid nanocrystals (0.06-0.50 mg/ml) were also investigated. As shown in Figure 8b, the temperature increase of the cyclohexane dispersions of the Ag-Ag_2S-CdS hybrid nanocrystal is 1.5-4.7 °C in 5 min. The rate of temperature increase gradually slows down with the irradiation time increase due to faster heat loss at higher temperature. In addtion, the temperature changes (ΔT) in 5 min, which are calculated from Figure 8b, go up dramatically with the increasing of Ag-Ag_2S-CdS concentrations from 0.06 to 0.12 mg/mL, and then exhibit a relatively flat upon further increasing the concentration to 0.5 mg/mL (shown in Figure SI-14, see SI). This phenomenon should be attributed to a fast heat loss at relatively high temperature, although the dispersion of Ag-Ag_2S-CdS hybrid nanocrystals with higher concentration (> 0.12 mg/mL) can absorb more photons of 980 nm.

For the widely reported noble metal-based materials, the photothermal conversion mechnism derives from the well-known localized surface plasmon resonance, in which most of the absorbed energy by metal nanoparticles releases as heat through the relaxation of surface currents.[75, 76, 77] The photothermal conversion mechanism of semiconductor (such as the prepared hybrid nanocrystals, silicon) [30, 33, 77, 78] is similar to that of carbon-based and organic compound-based photothermal agents. It is believed that heat is generated during the de-excitaion process after they were optically excited with an appropriate irradiaiton. The excitation state relax back to the ground state by radiative (with photoluminescence or phosphorescence) and/or non-radiative processes. In the non-radiative process, heat is produced due to phonon-assisted electronic decay and/or relaxation of free-carrier surface currents.[77-79]

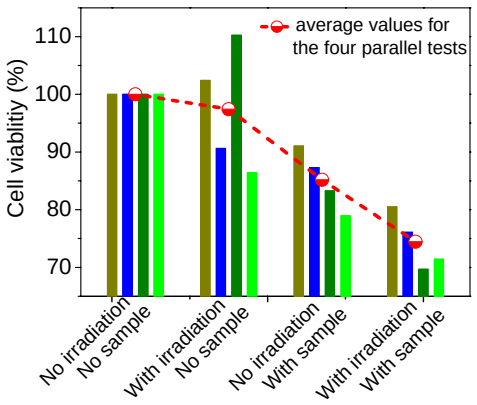

Fig. 9 Cell viabilities were estimated by the MTT proliferation tests, which was carried out with four parallel tests noted by four different colored columns.

The presence of heterointerfaces in nanocrystals usually induces the decreasing or quenching of fluorescence emission, thus more absorbed energy would deliver by heat. For the prepared Ag_2S-CdS nanocrystals with unique interlacedly microstructure, multiple Ag_2S/CdS heterointerfaces exist in one particle, thus relatively weak fluorescence emission and stronger photothermal conversion is observed in this sample (Figure 8b; Figure SI-12). While the heterointerfaces in the hybrid Ag-Ag_2S-CdS nanoparticle are relatively small, thus, the temperature increase is smaller than that of the Ag_2S-CdS product, although Ag nanocrystals are attached on them.

The hybrid nanocrystals as photothermal agent to destroy cancer cells were primarily evaluated *in vitro*. The ternary hybrid nanocrystal, Ag-Ag_2S-CdS, was selected as a representative sample for the test. Colon carcinoma cells in 96-well plates were used as a model of human tumor tissues to investigate the *in vitro* photothermal conversion capability (Figure 9). In order to get a reliable result, the evaluation and contrast experiments were both carried out in four parallel tests. All the results and the average values are shown in Figure 9. It can be seen that no apparent cancer cell death is observed upon treatment only with 980 nm photo-irradiation with power of 0.5 W (without Ag-Ag_2S-CdS). While a small part of the cells are dead when they are treated with the hybrid nanocrystals, Ag-Ag_2S-CdS, suggesting their possible cytotoxicity. In contrast, about 30 % cells die upon with photo-irradiation in the presence of hybrid nanocrystals. The increased cell death should be attributed to the photothermal effects of Ag-Ag_2S-CdS nanocrystals, since only small part of cells die with 980 nm laser or Ag-Ag_2S-CdS nanocrystals. Further study should be on the surface modification of the hybrid nanoparticles for decreasing the possible cytotoxicity, which is a common and open question for the nanoparticles used in bio-related field.[33] Although systematical toxicity examination and suitable surface modification research are needed, our preparation and preliminary property investigation results indicate a possible route for design a photothermal agent by introducing heterointerfaces.

Conclusions

In summary, a one pot and one-step route was developed for the synthesis of three-component Ag-Ag_2S-CdS hybrid nanocrystals. The hybrid nanocrystals with a size of 15.6 nm show uniform cubic shape and good monodispersity, and can be assembled into high ordered superstructure. It is revealed that the formation of Ag-Ag_2S-CdS hybrid nanocrystals is self-regulated and follows the sequence, Ag_2S, Ag, CdS. Partial reduction of Ag_2S and catalytic growth are responsible for the formation of Ag, CdS phase in the reaction system. The growth of CdS catalyzed by Ag_2S phase induces the structural transformation forming cubic hybrid nanocrystals. The Ag-Ag_2S-CdS hybrid nanocrystals combine NIR emission and photothermal conversion properties. When they were evaluated as photothermal conversion agent under the irradiation of 980 nm laser, the hybrid nanocrystals manifest enhanced photothermal conversion compared with their individual counterparts, which may be ascribed to the synergistic effect between them. The hybrid nanocrystals as photothermal agent to destroy cancer cells was also primarily evaluated *in vitro*. Thus, the research provided here would give a hint for design of advanced functional materials used in fields such as photothermal conversion agent.

Acknowledgements

The authors are grateful for financial support from National Natural Science Foundation of China (No. 51102117, 51203069), China Postdoctoral Science Foundation (2011M500085, 2012T50439), Jiangsu Postdoctoral Science Foundation (1102001C), Jiangsu Natural Science Foundation of China (No. BK2012276), and Cultivating Project of Young Academic Leader from Jiangsu University. Thanks to Dr. Rongxian Zhang and Dr. Wenhao Guo for their help in the *in vitro* test.

Notes and references

[a] School of Chemistry and Chemical Engineering, Jiangsu University, Zhenjiang 212013, P. R. China, E-mail: zhuguoxing@ujs.edu.cn; xiaopingshen@163.com; Fax: (+86)511-88791800; Tel: (+86)511-84401889

[b] School of Materials Science and Engineering, Jiangsu University, Zhenjiang 212013, P. R. China.

[c] School of Biology and Chemical Engineering, Jiangsu University of Science and Technology, Zhenjiang 212013, P. R. China.

[d] State Key Laboratory of Coordination Chemistry, Nanjing University, Nanjing 210093, P. R. China.

† Electronic Supplementary Information (ESI) available: TEM and HRTEM images, size distribution, and EDS patterns of some samples. See DOI: 10.1039/b000000x/

1 R. Costi, A. E. Saunders, U. Banin, *Angew. Chem. Int. Ed.*, 2010, **49**, 4878.
2 M. R. Buck, J. F. Bondi, R. E. Schaak, *Nature Chem.*, 2012, **4**, 37.
3 T. Teranishi, M. Sakamoto, *J. Phys. Chem. Lett.*, 2013, **4**, 2867.
4 T. Mokari, E. Rothenberg, I. Popov, R. Costi, U. Banin, *Science*, 2004, **304**, 1787.
5 N. N. Zhao, J. Vickery, G. Guerin, J. I. Park, M. A. Winnik, E. Kumacheva, *Angew. Chem. Int. Ed.*, 2011, **50**, 4606.
6 J. S. Beveridge, M. R. Buck, J. F. Bondi, R. Misra, P. Schiffer, R. E. Schaak, M. E. Williams, *Angew. Chem. Int. Ed.*, 2011, **50**, 9875.
7 P. Li, Z. Wei, T. Wu, Q. Peng, Y. D. Li, *J. Am. Chem. Soc.*, 2011, **133**, 5660.
8 J. Yang, J. Y. Ying, *Angew. Chem. Int. Ed.*, 2011, **50**, 4637.
9 H. M. Wu, O. Chen, J. Q. Zhuang, J. Lynch, D. LaMontagne, Y. Nagaoka, Y. C. Cao, *J. Am. Chem. Soc.*, 2011, **133**, 14327.
10 S. L. Xiong, B. J. Xi, K. Zhang, Y. F. Chen, J. W. Jiang, J. Y. Hu, H. C. Zeng, *Scientific Rep.*, **3**, 2177.
11 B. Liu, Z. F. Ma, *Small*, 2011, **7**, 1587.
12 M. D. Regulacio, C. Ye, S. H. Lim, M. Bosman, L. Polavarapu, W. L. Koh, J. Zhang, Q. H. Xu, M. Y. Han, *J. Am. Chem. Soc.*, 2011, **133**, 2052.

13 K. W. Kwon, M. Shim, *J. Am. Chem. Soc.*, 2005, **127**, 10269.
14 R. D. Robinson, B. Sadtler, D. O. Demchenko, C. K. Erdonmez, L. W. Wang, A. P. Alivisatos, *Science*, 2007, **317**, 355.
15 A. L. Rogach, A. Eychmuller, S. G. Hickey, S. V. Kershaw, *Small*, 2007, **3**, 536.
16 E. S. Shibu, M. Hamada, N. Murase, V. Biju, *J. Photochem. Photobio. C-Photochem. Rev.*, 2013, **15**, 53.
17 Q. W. Tian, J. Q. Hu, Y. H. Zhu, R. J. Zou, Z. G. Chen, S. P. Yang, R. W. Li, Q. Q. Su, Y. Han, X. G. Liu, *J. Am. Chem. Soc.*, 2013, **135**, 8571.
18 W. R. Chen, R. L. Adamsc, R. Carubellic, R. E. Nordquist, *Cancer Lett.*, 1997, **115**, 25.
19 Y. T. Lim, S. Kim, A. Nakayama, N. E. Scott, M. G. Bawendi, J. V. Frangioni, *Mol. Imaging*, 2003, **2**, 50.
20 L. Bakueva, I. Gorelikov, S. Musikhin, X. S. Zhao, E. H. Sargent, E. Kumacheva, *Adv. Mater.*, 2004, **16**, 926.
21 Z. Chen, S. M. Tabakman, A. P. Goodwin, M. G. Kattah, D. Daranciang, X. R. Wang, G. Y. Zhang, X. L. Li, Z. Liu, P. J. Utz, K. L. Jiang, S. S. Fan, H. J. Dai, *Nat. Biotechnol.*, 2008, **26**, 1285.
22 L. Aboshyan-Sorgho, H. Nozary, A. Aebischer, J. G. Bünzli, P. Morgantini, K. R. Kittilstved, A. Hauser, S. V. Eliseeva, S. Petoud, C. Piguet, *J. Am. Chem. Soc.*, 2012, **134**, 12675.
23 Y. P. Gu, R. Cui, Z. L. Zhang, Z. X. Xie, D. W. Pang, *J. Am. Chem. Soc.*, 2012, **134**, 79.
24 C. M. Andolina, A. C. Dewar, A. M. Smith, L. E. Marbella, M. J. Hartmann, J. E. Millstone, *J. Am. Chem. Soc.*, 2013, **135**, 5266.
25 E. Boisselier, D. Astruc, *Chem. Soc. Rev.*, 2009, **38**, 1759.
26 V. S. Thakare, M. Das, A. K. Jain, S. Patil, S. Jain, *Nanomedicine*, 2010, **5**, 1277.
27 Y. Xia, W. Li, C. M. Cobley, J. Chen, X. Xia, Q. Zhang, M. Yang, E. C. Cho, P. K. Brown, *Acc. Chem. Res.*, 2011, **44**, 914.
28 M. S. Yavuz, Y. Cheng, J. Chen, C. M. Cobley, Q. Zhang, M. Rycenga, J. Xie, C. Kim, K. H. Song, A. G. Schwartz, L. V. Wang, Y. Xia, *Nature Mater.*, 2009, **8**, 935..
29 X. Q. Huang, S. H. Tang, X. L. Mu, Y. Dai, G. X. Chen, Z. Y. Zhou, F. X. Ruan, Z. L. Yang, N. F. Zheng, *Nat. Nanotechnol.*, 2011, **6**, 28.
30 Q. Tian, M. Tang, Y. Sun, R. Zou, Z. Chen, M. Zhu, S. Yang, J. H. Wang, J. L. Wang, J. Q. Hu, *Adv. Mater.*, 2011, **23**, 3542.
31 H. Liu, D. Chen, L. Li, T. Liu, L. Tan, X. Wu , F. Tang, *Angew. Chem. Int. Ed.*, 2011, **50**, 891.
32 X. Wang, C. Wang, L. Cheng, S. T. Lee, Z. Liu, *J. Am. Chem. Soc.*, 2012, **134**, 7414.
33 G. S. Song, Q. Wang, Y. Wang, G. Lv, C. Li, R. J. Zou, Z. G. Chen, Z. Y. Qin, K. K. Huo, R. G. Hu, J. Q. Hu, *Adv. Funct. Mater.*, 2013, **23**, 4281.
34 M. A. Hahn, A. K. Singh, P. Sharma, S. C. Brown, B. M. Moudgil, *Anal. Bioanal. Chem.*, 2011, **399**, 3.
35 X. J. Song, H. Gong, S. N. Yin, L. Cheng, C. Wang, Z. W. Li, Y. G. Li, X. Y. Wang, G. Liu, Z. Liu, *Adv. Funct. Mater.*, 2014, **24**, 1194.
36 W. P. Lim, Z. Zhang, H. Y. Low, W. S. Chin, *Angew. Chem. Int. Ed.*, 2004, **43**, 5685.
37 J. H. Xiang, H. Q. Cao, Q. Z. Wu, S. C. Zhang, X. R. Zhang, A. A. R. Watt, *J. Phys. Chem. C*, 2008, **112**, 3580.
38 Y. P. Du, B. Xu, T. Fu, M. Cai, F. Li, Y. Zhang, Q. B. Wang, *J. Am. Chem. Soc.*, 2010, **132**, 1470.
39 Y. Zhang, G. S. Hong, Y. J. Zhang, G. C. Chen, F. Li, H. J. Dai, Q. B. Wang, *ACS Nano*, 2012, **6**, 3695.
40 G. X. Zhu, Z. Xu, *J. Am. Chem. Soc.*, 2011, **133**, 148.
41 W. W. Xu, J. Z. Niu, H. Z. Wang, H. B. Shen, L. S. Li, *ACS Applied Materials & Interf.*, 2013, **5**, 7537.
42 J. L. Wang, K. M. Chen, M. Gong, B. Xu, Q. Yang, *Nano Lett.*, 2013, **13**, 3996.
43 A. K. Guria, S. Sarkar, B. K. Patra, N. Pradhan, *J. Phys. Chem. Lett.*, 2014, **5**, 732.
44 R. Bose, G. Manna, S. Jana, N. Pradhan, *Chem. Comm.*, 2014, **50**, 3074.
45 Z. P. Huang, M. Y. Li, D. Jia, P. Zhong, F. Tian, Z. Z. Chen, M. G. Humphrey, C. Zhang, *J. Mater. Chem. C*, 2014, **2**, 1418.
46 D. S. Wang, C. H. Hao, W. Zheng, Q. Peng, T. H. Wang, Z. M. Liao, D. P. Yu, Y. D. Li, *Adv. Mater.*, 2008, **20**, 2628.
47 M. Han, S. Liu, X. Nie, D. Yuan, P. Sun, Z. Dai, J. C. Bao, *RSC Adv.*, 2012, **2**, 6061.
48 B. V. R. Chowdari, K. F. Mok, J. M. Xie, R. Gopalakrishnan, *J. Non-Cryst. Solids*, 1993, **160**, 73.
49 F. X. Xiao, J. W. Miao, B. Liu, *J. Am. Chem. Soc.*, 2014, **136**, 1559.
50 V. G. Bhide, S. Salkalachen, A.C. Rastogi, C. N. R. Rao, M. S. Hegde, *J. Phys. D.*, 1981, **14**, 1647.
51 C. D. Wagner, A. V. Naumkin, A. Kraut-Vass, J. W. Allison, C. J. Powell, J. R. Rumble, *NIST X-ray photoelectron spectroscopy database*, 2003, Version 3.3.
52 J. Zhang, J. G. Yu, M. Jaroniec, J. R. Gong, *Nano Lett.*, 2012, **12**, 4584.
53 A. M. Ferraria, A. P. Carapeto, A. M. B. Rego, *Vacuum*, 2012, **86**, 1988.
54 J. F. Moulder, W. F. Stickle, P. E. Sobol, K. D. Bomben, *Handbook of Standard Spectra for Identification and Interpretation of XPS Data*, Perkin Elmer Corporation, 120.
55 E. Erasmus, P. C. Thüne, M. W. G. Verhoeven, J. W. Niemants-verdriet, J. C. Swarts, *Catal. Commun.*, 2012, **27**, 193.
56 C. Carolina, B. J. Carlos, B. M. L. Zapata, Z. J. Manuel, *Microp. Mesop. Mater.*, 2014, **188**, 118.
57 M. L. Pang, J. Y. Hu, H. C. Zeng, *J. Am. Chem. Soc.*, 2010, **132**, 10771.
58 L. Motte, J. Urban, *J. Phys. Chem. B*, 2005, **109**, 21499.
59 A. I. Kryukov, A. L. Stroyuk, N. N. Zinchuk, A. V. Korzhak, S. Y. Kuchmii, *J. Mole. Catal. A-Chem.*, 2004, **221**, 209.
60 H. Liu, W. W. Hu, F. Ye, Y. L. Ding, J. Yang, *RSC Adv.*, 2013, **3**, 616.
61 Y. Xu, M. A. A. Schoonen, *Am. Mineral.*, 2000, **85**, 543.
62 D. R. Lide, *CRC Handbook of Chemistry and Physics*, 87-th edn, CRC Press, 2006.
63 S. J. Tauster, S. C. Fung, R. T. K. Baker, J. A. Horsley, *Science*, 1981, **211**, 1121.
64 S. J. Tauster, *Acc. Chem. Res.*, 1987, **20**, 389.
65 M. Kobayashi, *Solid State Ionics*, 1990, **39**, 121.
66 M. Sheldon, P. Trudeau, T. Mokari, L. Wang, A. P. Alivisatos, *Nano Lett.*, 2009, **9**, 3676.
67 P. Rukenstein, I. J. Plante, M. Dia, E. Chockler, K. Flomin, B. Moshofsky, T. Mokari, *CrystEngComm*, 2012, **14**, 7590.
68 Y. X. Zhao, Z. M. Song, *Mater. Lett.*, 2014, **126**, 78.

69 H. Meherzi-Maghraoui, M. Dachraoui, S. Belgacem, K. D. Buhre, R. Kunst, P. Cowache, D. Lincot, *Thin Solid Films*, 1996, **288**, 217.
70 S. L. Shen, Y. L. Zhang, L. Peng, Y. P. Du, Q. B. Wang, *Angew. Chem. Int. Ed.*, 2011, **50**, 7115.
71 R. Weissleder, *Nat. Biotechnol.*, 2001, **19**, 316.
72 L. Zhuang, S. Tabakman, K. Welsher, H. J. Dai, *Nano Res.*, 2009, **2**, 85.
73 N. W. S. Kam, M. J. O'Connell, J. A. Wisdom, H. Dai, *Proc. Natl. Acad. Sci.*, 2005, **102**, 11600.
74 V. Shanmugam, S. Selvakumarb, C. S. Yeh, *Chem. Soc. Rev.*, 2014, DOI: 10.1039/c4cs00011k.
75 H. J. Chen, L. Shao, T. Ming, Z. H. Sun, C. M. Zhao, B. C. Yang, J. F. Wang, *Small*, 2010, **6**, 2272.
76 D. Jaque, L. M. Maestro, B. Rosal, P. Haro-Gonzalez, A. Benayas, J. L. Plaza, E. M. Rodríguez, J. G. Solé, *Nanoscale*, 2014, DOI: 10.1039/c4nr00708e.
77 L. Maestro, P. Haro-González, J. Coello, D. Jaque, *Appl. Phys. Lett.*, 2012, **100**, 201110.
78 C. Lee, H. Kim, C. Hong, M. Kim, S. S. Hong, D. H. Lee, W. I. Lee, *J. Mater. Chem.*, 2008, **18**, 4790.
79 C. M. Hessel, V. P. Pattani, M. Rasch, M. G. Panthani, B. Koo, J. W. Tunnell, B. A. Korgel, *Nano Lett.*, 2011, **11**, 2560.